Journal of Physics Communications

OPEN ACCESS

RECEIVED
10 December 2019

REVISED
18 March 2020

ACCEPTED FOR PUBLICATION
27 March 2020

PUBLISHED
9 April 2020

PAPER

A systematic computational study of electronic, mechanical, and optical properties of $Fe_{1-x}Co_x$ alloy

Ali Hossain , M Khalilur Rahman Khan and Md Samiul Islam Sarker

Department of Physics, University of Rajshahi, Rajshahi-6205, Bangladesh

E-mail: samiul-phy@ru.ac.bd

Keywords: spin polarization, elastic constant, optical properties, plasmonic resonance

Abstract

This report demonstrates the systematic study of electronic, mechanical, and optical properties of $Fe_{1-x}Co_x$ alloy (x = 0.00, 0.05, 0.10, 0.15, 0.20, and 0.25) using plane wave ultrasoft pseudopotential based on spin-polarized density functional theory. The upshots expose overlapped of valence and conductance states and confirms electronic bands polarization. The energy bands are significantly shifted with increasing Co atoms. The dispersion energies reveal anisotropic behavior of electronic energy levels. The density of states manifests strong electronic interaction between Co and Fe atoms. The spin polarization is mainly attributed from the exchange interactions among electronic spins, which confirms the strong electron-electron interactions. Subsequently, spin polarization induces spin magnetic moments. Minority spin states are dominant for $Fe_{1-x}Co_x$ alloy, which significantly changed the electronic properties. Moreover, Elastic constants confirm that all the phases of $Fe_{1-x}Co_x$ alloy are mechanically stable, and the higher elastic modulus manifests better performance of the resistance to shape change and against uniaxial tensions. The optical properties of FeCo alloy exhibit strong interrelation with atomic composition of Fe and Co. The loss spectra reveal high plasmonic resonance that can be chemically tuned through atomic composition. The spin magnetic moments and high plasmonic resonance make the $Fe_{1-x}Co_x$ alloys as the prominent mechanically stable materials for magneto-optical applications.

1. Introduction

Spin-polarized computations within the framework of density-functional theory (DFT) are a powerful technique to understand the electronic structure of transition metals. The fundamental development of spin density functional theory by Barth *et al* and Pant *et al* are reported [1, 2]. The transition metals (Fe, Co, and Ni) alloys and compounds have seemed as materials of extensive importance and opened up significant scopes in many fields of materials science and engineering [3]. The spin polarized DFT can illustrate remarkable picture of electronic exchange-correlation owing to spin interactions of alloys. Though the alloys have no band-gap, however, the electronic energy levels exhibit significant change in position in Brillouin zone as well as in Fermi level for various concentrations.

FeCo alloys have greater attraction due to its rich physical and chemical properties. Such as ferroelectricity at room temperature, high Curie temperature, high magnetic moments, and mechanical hardness, etc For these properties, FeCo alloy can be promoted for various technological applications for instance, transformer core, electric motor, pole-pieces, high density magnetic recording, biomedicine, drug delivery, magnetic resonance imaging, magnetic hyperthermia and specially data storage and so on [4–11]. Elasticity is the embryonic property of solid materials that is essential in numerous areas spanning of materials selection in mechanical design. In addition, the elastic property is important to build up relationship between materials deformation and stress. The elastic anisotropy of solid materials is the dependency of elastic modulus. The anisotropic behaviors of solid materials have an important implication in engineering science and technology as well as condensed matter physics.

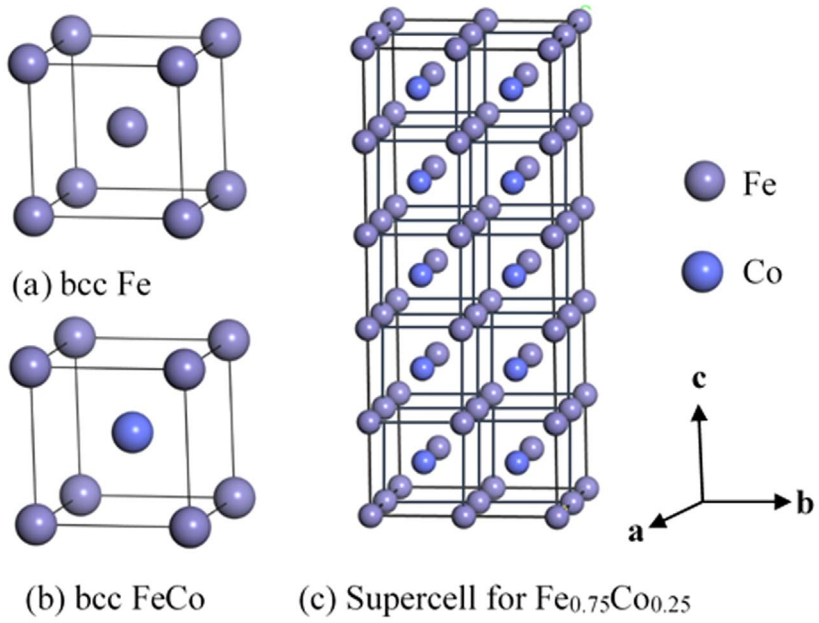

Figure 1. Crystal structures of (a) bcc Fe, (b) bcc FeCo, and (c) $Fe_{0.75}Co_{0.25}$ supercell.

Many experimental research have been performed on structural and magnetic properties of FeCo alloys [10, 12, 13]. However, based on composition, only a very few computational studies have focused on electronic, magnetic, and mechanical properties. In addition to that the optical properties are rarely reported. For example the electronic properties of ordered-disordered FeCo binary alloy have been reported through various approximations such as coherent potential approximation (CPA) and local spin density approximation (LSDA), tight binding approach, linear combination of atomic orbitals theory in combination with CPA methods etc [10, 14, 15]. The calculated elastic constant through approximation of tight binding recursion using Born-Mayer repulsive potential, electron exact muffin-tin orbitals method in combination with the CPA and DFT methods are found in literature [14–16]. The FeCo alloy is considered as chemically disordered materials and it manifests peculiar physical and chemical properties through possessing different atomic composition.

In this study, we have demonstrated the electronic structure, mechanical, and more importantly the optical properties of the $Fe_{1-x}Co_x$ alloy ($x = 0.00, 0.05, 0.10, 0.15, 0.20$, and 0.25) by substituting Co atom on body-centered cubic Fe crystal. The electronic structure has been computed using spin polarized DFT through generalized gradient approximation (GGA) approached plane wave ultrasoft pseudopotential. The density of states (DOS) demonstrates the spin-electronic exchange interaction critically. The large spin interaction appears for highly disordered alloys and shows induced spin magnetic moments. The elastic constants, bulk modulus, shear modulus, Young's modulus, Poisson's ratio and anisotropic factor have also been presented through stress-strain technique. The optical loss spectra manifest large optical kerr effect owing to bulk plasmonic resonance at the material dielectric interface. The plasmonic resonance frequency of $Fe_{1-x}Co_x$ alloys can be tuned chemically through controlling atomic composition, which makes the $Fe_{1-x}Co_x$ alloy as a suitable material for magneto-optical applications.

2. Crystal modelling

The electronic, mechanical, and optical properties of $Fe_{1-x}Co_x$ alloys have been computed through first principles techniques based on density functional theory employed in Cambridge serial total energy package (CASTEP) code [17]. The crystallographic structural unit cell of FeCo alloy is body-centered cubic (bcc) in which the Fe atoms occupied primitive cubic sites and Co atom appears at the center of the unit cell. In these computations, $2 \times 2 \times 5$ supercell of bcc Fe have been used and Fe atoms substituted by Co atoms systematically to optimize the ground state energies of disordered $Fe_{1-x}Co_x$ alloy ($x = 0.00, 0.05, 0.10, 0.15$, 0.20 and 0.25) (figure 1). The supercell structure of $Fe_{0.75}Co_{0.25}$ is shown in figure 1(c). The energy cut-off and number of k-points have been used to measure how well one discrete grid has appointed the continuous integral. The interactions among valence electrons and ions are considered using the Vanderbilt type ultrasoft pseudopotential (UPP) formalism [18–20]. UPPs attain much softer pseudo-wave function, which considerably used fewer plane waves for calculations of the same accuracy. To obtain the ground state optimization, we have

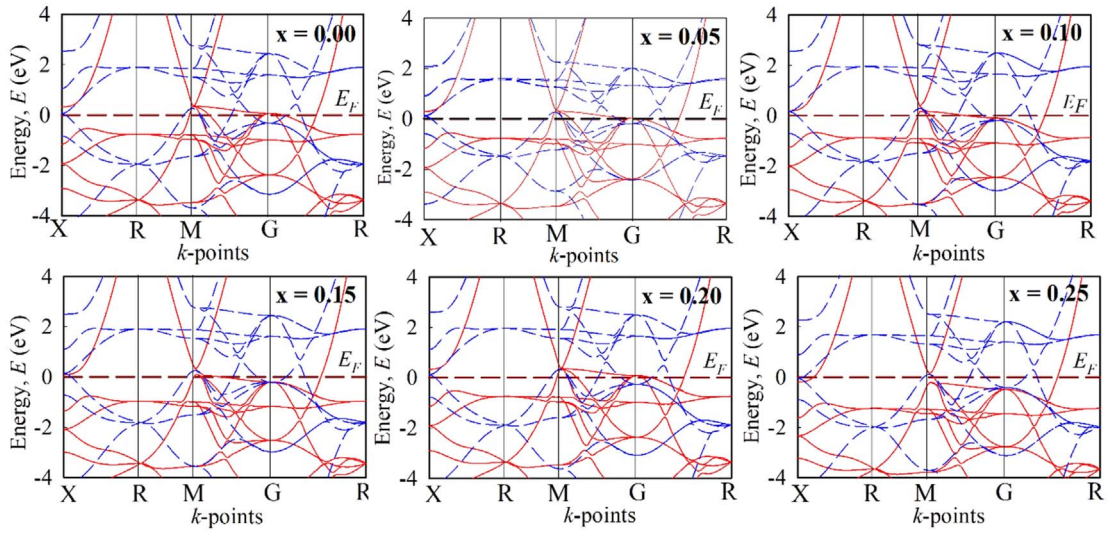

Figure 2. Band structures of $Fe_{1-x}Co_x$ alloy. Red solid line and blue dashed line indicate the energy levels due to up-spin and down-spin states, respectively.

utilized the Broyden-Fletcher-Goldfarb-Shanno (BFGS) minimization techniques [21]. The optimizations were performed through plane wave energy cut-off and Monkhorst–Pack [22] grid parameter for sampling of the Brillouin zone. The GGA of the Perdew–Burke–Ernzerhof (PBE) formalism is used to evaluate the exchange-correlation energy [23]. Optimization is operated using convergence thresholds of 10^{-5} eV/atom for the total energy and 10^{-3} Å for maximum displacement. Maximum force and stress are 0.03 eV $Å^{-1}$ and 0.05 GPa respectively for all the calculations. The elastic constants are carried out through 'stress-strain' techniques. The elastic properties such as the elastic constants, bulk modulus and shear modulus are computed as employed in CASTEP code. All computations have been carried out through zero applying pressure.

3. Results and discussion

3.1. Electronic structures

3.1.1. Band structures

The electronic band structures have been computed to understand the electronic behavior and the electronic dispersion properties of the $Fe_{1-x}Co_x$ alloys. The properties of the material can be understood by identifying the characteristics of dominant bands near the Fermi level, and their energy etc. The electronic energy bands of $Fe_{1-x}Co_x$ alloy along the high symmetry directions (X-R-M-G-R) of the Brillouin zone in the energy range from -4 to +4 eV are presented in figure 2. The Fermi level, E_F is taken as the reference point and set to zero at the energy scales. It is seen from figure 2, that the valence band and conduction band are overlapped that confirms the metallic-like behavior of the alloys [24].

The asymmetric formation of energy bands confirms that the electronic states are polarized. At X-point, the electronic states of disordered alloys shift to lower energy compared to x = 0.00 and consequently, electronic properties indicate down-spin dominant nature of the alloys. The electronic states are slightly shifted with increasing Co content. The G-point also exhibits the peculiar features of spin polarization of the electronic bands. The dispersion along G-point is highly asymmetric. In addition, the band structure shows strongly anisotropic features with characteristics energy dispersion along the axial axes. The electronic dispersion along M-G directions is more complex than that of X-R directions. The electrical conductivity is anisotropic for these alloys, i.e., the electrical conductivity owns different values in each crystal plane [10].

3.1.2. Density of states (DOS)

The DOS manifests the number of electronic states per unit energy interval. All calculations carried out by choosing Fermi level position as the reference point. The DOS of $Fe_{1-x}Co_x$ alloy is shown in figure 3. It is seen from figure 3, that the DOS exhibits non-zero values at Fermi level, E_F. These non-zero values of DOS manifest the overlap of valence band and conduction band. Thus, $Fe_{1-x}Co_x$ alloy reveals the metallic nature which is expected for this type of bimetallic alloy [10, 24, 25]. Moreover, the spin densities around the Fermi level possess some values that demonstrates the polarization of these bands as well that also attests the energy dispersion along the polarization direction as shown in band diagram (figure 2). Spin magnetic moments are induced due to

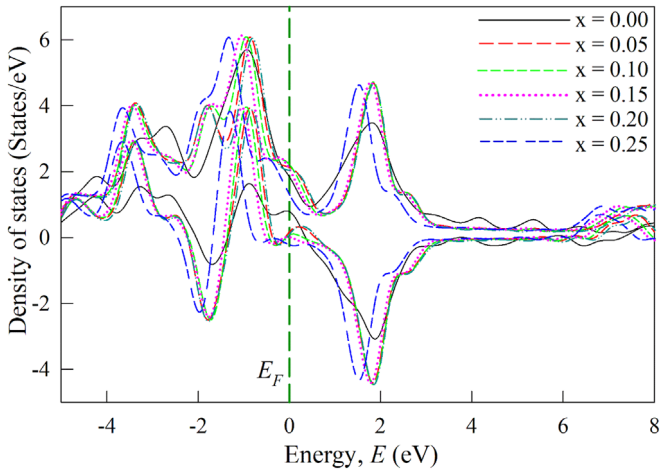

Figure 3. Density of states of $Fe_{1-x}Co_x$ alloy as a function of energy. The total DOS are plotted in positive scale and negative scale is taken for spin DOS. The vertical long dashed line indicates the Fermi level, E_F.

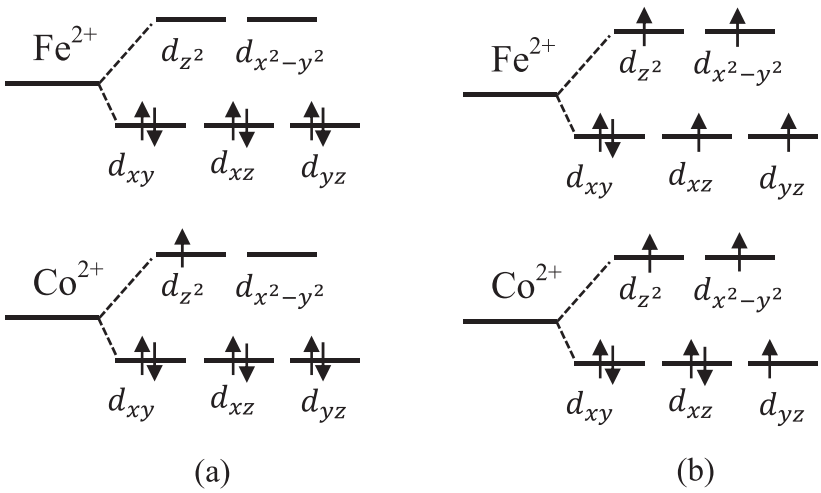

Figure 4. Schematic spin orientations of Fe^{2+} and Co^{2+} ions, (a) low spin states and (b) high spin states.

Table 1. Total density of states, spin densities and spin magnetic moments of $Fe_{1-x}Co_x$ alloy.

Concentration of Co, x	TDOS (States/eV)	Up-spin DOS (States/eV)	Down-spin DOS (States/eV)	Spin magnetic moments (μ_B)
0.00	1.86	1.32	0.53	1.48
0.05	2.13	1.18	0.56	1.27
0.10	2.20	1.15	1.04	0.48
0.15	2.07	1.03	1.02	0.14
0.20	2.08	1.13	0.94	0.64
0.25	1.26	0.51	0.75	0.73

polarization of these energy bands. The DOS around the Fermi level mainly comes from hybridization of 3d electronic orbitals of Fe and Co atoms. The total and spin DOS are tabulated in table 1.

The total DOS increases with increasing Co concentrations up to 0.10, then it decreases (table 1). According to crystal field theory, hybridized d-orbital d_{z^2} and $d_{x^2-y^2}$ possess higher energy than d_{xy}, d_{xz}, d_{yz} and repels each other. A geometrical spin orientations Fe^{2+} and Co^{2+} are shown in figure 4. It is seen that the d_{z^2} and $d_{x^2-y^2}$ orbitals are unoccupied for Fe low spin states, while Co has one more up-spin electron than Fe. Besides, the all orbitals are occupied in high spin states and Fe^{2+} has one more spin than Co^{2+}. The bcc Fe and Co are atomically

Table 2. The elastic constants, bulk modulus, B shear modulus, G Young's modulus, Y (all are in GPa), G/B ratio, Poisson's ratio, ν and anisotropy factor, A of $Fe_{1-x}Co_x$ alloy.

x	C_{11}	C_{12}	C_{44}	B	G	Y	G/B	ν	A
0.00	295.67	159.03	126.12	204.57	98.61	254.88	0.48	0.29	1.85[a]
0.05	289.10	159.47	116.22	202.68	91.94	239.59	0.45	0.30	1.79
0.10	275.54	161.32	125.50	199.39	91.50	238.08	0.46	0.30	2.20
0.15	282.74	161.50	132.37	201.92	96.75	250.28	0.48	0.29	2.18
0.20	301.42	168.72	142.34	212.95	104.78	270.05	0.49	0.29	2.15
0.25	307.20	162.27	143.35	210.58	109.02	278.92	0.52	0.28	1.98

[a] [15].

saturated ferromagnets and Co has slightly higher electron negativity than Fe atoms. The local moment induces from intra-atomic exchange interactions between Fe and Co atoms. The electronic state splits and exchange interaction increases during the formation of $Fe_{1-x}Co_x$ alloy. At Co concentration, $x = 0.15$, the local moments of Co affect the minority states that indicates an electronic transition state. The crystal field is attributed at transition state and the electronic moments transform from low-spin to high-spin states owing to direct repulsion of the d_{z^2} and $d_{x^2-y^2}$ orbitals [3]. Consequently, electronic state increases, but the spin magnetic moment decreases. The spin magnetic moment is determined from the dissimilarity of the up-spin and down-spin states, which indicates the ferromagnetic nature of the $Fe_{1-x}Co_x$ alloys as shown in figure 3. The high spin manifests the exchange interactions of electronic energy states and confirms strong electron-electron interactions. However, it is seen from table 1 that the total DOS decreases as well as spin magnetic moment increases with substituting Co content from 0.20 to 0.25, which can be explained by Stoner criteria of ferromagnetism [26]. The spin states of Fe and Co can be changed from low to high due to increasing degree of disordered of the crystal. According to Stoner criteria, exchange interaction decreases due to the dispersion relation between up-spin and down-spin electrons where the electron-electron interaction is disregarded.

3.2. Mechanical properties

The mechanical properties have been computed through determining elastic constants. The elastic constants, C_{ij} can be defined as the second derivatives of the ground state energy with respect to strain components. Any symmetry present in the structure may make some of these components equal and other may be fixed at zero. So, a cubic crystal has only three different symmetry elements (C_{11}, C_{12} and C_{44}), each of which represents three equal elastic constants ($C_{11} = C_{22} = C_{33}$; $C_{12} = C_{23} = C_{31}$; $C_{44} = C_{55} = C_{66}$). Nye reported a full account of the symmetry of stress, strain and elastic constants [27]. A single strain with non-zero first and fourth components can give stresses relating to all three of these coefficients, yielding a very efficient method for obtaining elastic constants for the cubic system. The elastic constants described the response of a material to an applied stress. They provide a link between the mechanical and dynamic information concerning the nature of the forces operating in solids, especially for the stability and stiffness of materials [28, 29]. The mechanically stable phases or macroscopic stability are dependent on the positive definiteness of stiffness matrix. For the stability of cubic lattices, the following conditions known as the Born criteria [30] must be carried out: $C_{11} > 0$, C_{11}–$C_{12} > 0$, $C_{44} > 0$. Our calculated elastic constants completely satisfy the above conditions, indicating that the all phases of $Fe_{1-x}Co_x$ alloy are mechanically stable. Further, the calculated bulk modulus, B and shear modulus, G allow us to obtain the Young's modulus, Y and the Poisson's ratio ν as $Y = 9BG/(3B + G)$ and $\nu = (3B - 2G)/2(3B + G)$ respectively. The elastic constants, bulk modulus, B shear modulus, G Young's modulus, Y (all are in GPa), G/B ratio, Poisson's ratio, ν and anisotropy factor, A of $Fe_{1-x}Co_x$ alloy have been tabulated in table 2. The calculated results are consistent with reported values [15]. The Young's modulus is defined as the ratio between stress and strain and is used to provide a measure of stiffness, i.e., the larger the value of Y, the stiffer the material. We noted that the Young's modulus, Y of possesses large values that shows a better performance of the resistance to shape change and against uniaxial tensions.

It is vivid from table 2 that, the materials become harder with increasing Co content. The ductility of a material can be roughly estimated by the ability of performing shear deformation, such as the value of shear-modulus to bulk-modulus ratios. Thus, a ductile plastic solid would show low G/B ratio (<0.5); otherwise, the material is brittle [31]. The calculated G/B ratio is less than o.5 except $x = 0.25$, for these investigated materials. So, the alloys are ductile plastic solid while $Fe_{0.75}Co_{0.25}$ is brittle.

Elastic anisotropy study is an important part for materials design. Therefore, it has a significant role in engineering science due to the possibility of creation and propagation of microcracks in the crystals. The elastic anisotropic factor is calculated as, $A = 2C_{44}/(C_{11} - C_{12})$. The anisotropic factors are well consistent and good

agreement with reported values [32, 33]. The anisotropy gives an account of the ratio of the extreme values of the orientation-dependent shear modulus.

3.3. Optical properties

The optical properties of materials can be described entirely by complex dielectric function $\varepsilon(\omega) = \varepsilon_1(\omega) + i\varepsilon_2(\omega)$, which correlated with interactions of photons and electrons at all frequencies. The imaginary part $\varepsilon_2(\omega)$ of dielectric function can be calculated from the momentum matrix elements between the occupied and unoccupied wave functions, which is given by,

$$\varepsilon_2(\omega) = \left(\frac{4\pi^2 e^2}{m^2\omega^2}\right)\sum_{i,j}\int i|M_d|\, j^2 f_i(1 - f_i)\delta(E_f - E_i - \omega)d^3k \tag{1}$$

where, M_d is the dipole matrix, i and j are the initial and final states, respectively, f_i is the Fermi distribution function for the i-th state, and E_i is the energy of electron in the i-th state. The real part $\varepsilon_1(\omega)$ of dielectric function can be evaluated from $\varepsilon_2(\omega)$ using Kramers-Kronig relations [34] as follows

$$\varepsilon_1(\omega) = 1 + \frac{2}{\pi}P\int_0^\infty \frac{\omega'\varepsilon_2(\omega')d\omega'}{(\omega'^2 - \omega^2)} \tag{2}$$

where, P implies the principal value of the integral. Optical parameters can be calculated from the knowledge of both the real and imaginary parts of the dielectric tensor. The optical parameters (dielectric function, refractive index, loss function, reflectivity, and extinction coefficient) of $Fe_{1-x}Co_x$ have been calculated as a function of incident photon energies up to 25 eV for [100] polarization direction. For the metallic compounds both inter-band and intra-band transitions contribute to dielectric functions. A Drude term with unscreened plasma frequency, 3 eV and damping, 0.05 eV has been used to enhance the low energy part of the spectrum.

The dielectric function explains how a material response to the electromagnetic radiation, in particular to visible light. Both the real and imaginary part of dielectric function are shown in figures 5(a) and (b), respectively as a function of incident photon energy. The dielectric function attests the metallic nature of the material as depicted earlier in section 3.1. The real part of dielectric function decreases with increasing photon energy up to ultraviolet region. The negative value of the real part of dielectric function reveals that it shows the intraband Drude-like characteristics. The imaginary part of dielectric constant shows characteristic peaks for disordered $Fe_{1-x}Co_x$ alloys at lower energy part. The peaks become wider with high Co content and it indicates the optical transition between Fe (3d) to Co (3d) states. At high energy region, the real part of dielectric function becomes almost constant and the value of imaginary part possesses very close to zero. It manifests itself the material is optically anisotropic. The dielectric formalism is mainly arises from electronic polarization. The simulated reflectivity for different concentration of $Fe_{1-x}Co_x$ alloy are presented in figure 5(c). The reflectivity of the disordered $Fe_{1-x}Co_x$ alloys are slightly increasing with substituting Co atoms up to ~20 eV. The real part of refractive index determines the phase velocity and the imaginary part determines the amount of absorption loss when an electromagnetic wave passes through the materials. It is seen in figure 5(d) that the real part of refractive index sharply decreased in low energy region up to 5 eV. Moreover, extinction coefficient linearly increased at low energy region and shows characteristics peaks at ~4.2 eV as shown in figure 5(e). Then it decreases that indicates how incident energy absorbed in the materials. The maximum extinction coefficients found for $x = 0.25$ Co content.

The computed energy loss spectra are shown in figure 5(f). The energy loss spectra of materials are very important parameter in the dielectric formalism, which is useful to understand the screened excitation spectra, especially the collective excitations produced by the swift charges inside the solid. Loss function refers to the fast electron traversing in a material. Hence, the loss function analysis is most important in materials study. The highest peak of the energy loss spectrum appears due to bulk plasmonic excitation at a particular incident photon energy as well as the corresponding frequency known as the bulk plasma frequency. The loss function is correlated with optical reflectivity. The bulk plasmonic excitation appears at the corresponding energies, where material exhibits highest reflectivity. In loss spectrum, the plasmonic resonance frequency is located at 20 eV for $x = 0$. The loss spectrum reveals quite different picture for disordered $Fe_{1-x}Co_x$ alloys. The plasmonic resonance frequency becomes shifted left with increasing substitution of Co atoms. It indicates the plasmonic excitations at the metal-dielectric interface due to optical transition of Co/Fe electrons from p to d states instead of absorbing high energy photons. For $Fe_{0.75}Co_{0.25}$, bulk plasmonic excitation appears at 19.2 eV with high loss function than Fe. These types of loss spectroscopy manifests that the material is applicable for guiding of light below the diffraction limit (near-field optics), non-linear optics, biosensors etc [35]. In addition, the peaks of loss spectrum indicate the large magneto-optical kerr effect (MOKE) which is expected for high density magneto-optical devices [36].

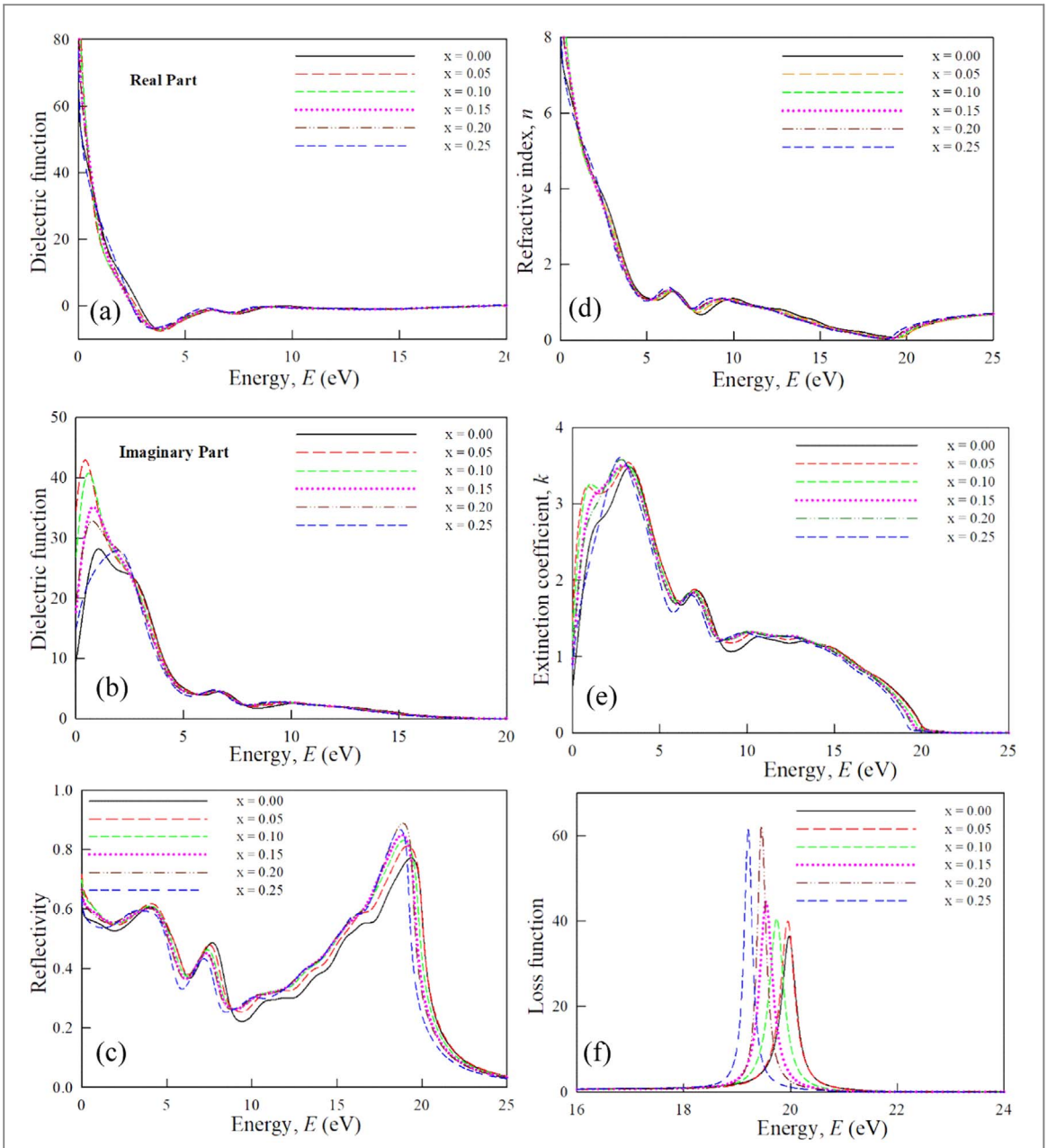

Figure 5. Calculated optical parameters (a) real part of dielectric function, (b) imaginary part of dielectric function, (c) reflectivity, (d) refractive index, (e) extinction coefficient, and (f) loss function as function of incident photon energy, E (eV).

4. Conclusions

The effects of composition on the electronic structures, mechanical, and optical properties of disordered $Fe_{1-x}Co_x$ alloy with x = 0.00, 0.05, 0.10, 0.15, 0.20, and 0.25 have been reported through plane wave ultrasoft pseudopotential approached spin-polarized density functional theory. The density of states manifests strong electron-electron interactions and polarization of electronic states. The electronic states are polarized due to exchange interactions of spins and induce spin magnetic moments. The high spin configuration appears with increasing Co content. The high spin moment makes the $Fe_{1-x}Co_x$ alloys as a promising candidate for magnetic valves, magnetic random access memory, solid state capacitor and so on. Moreover, the $Fe_{1-x}Co_x$ alloys are mechanically anisotropic. The calculated elastic modulus shows the materials are stiffer with increasing Co content. The results are well consistent with reported theoretical and experimental values. In addition, the optical parameters are significantly changed with atomic composition. The bulk plasmonic resonance frequency of $Fe_{1-x}Co_x$ alloys can be tuned chemically through controlling atomic composition, which makes the $Fe_{1-x}Co_x$ alloy as a suitable material for magneto-optical applications.

ORCID iDs

Ali Hossain https://orcid.org/0000-0001-6201-5978
Md Samiul Islam Sarker https://orcid.org/0000-0002-5399-6150

References

[1] Barth U V, Hedin L, Phys. J and Solid C 1972 *States Phys.* **5** 1629
[2] Pant M M and Rajagopal A K 1972 *Solid State Commun.* **10** 1157
[3] Hossain A, Sarker M S I, Khan M K R and Rahman M M 2020 *Materials Science & Engineering* B **253** 114496
[4] Kumar C and Mohammad F 2011 *Adv. Drug Deliv. Rev.* **63** 789
[5] Habib A H, Ondeck C L, Chaudhary P, Bockstaller M R and McHenry M E 2008 *J. Appl. Phys.* **103** 07A307
[6] Thirumal E, Prabhu D, Chattopadhyay K and Ravichandran V 2010 *Phys. Status Solidi a* **207** 2505
[7] Shokuhfar A and Afghahi S S S 2013 *Nanoscale Res. Lett.* **8** 540
[8] Lee S J, Cho J H, Lee C, Cho J, Kim Y R and Park J K 2011 *Nanotechnology* **22** 375603
[9] Hossain A, Sarker M S I, Khan M K R and Rahman M M 2018 *J. Phys. Conf. Ser.* **1086** 012004
[10] Zehani K *et al* 2014 *J. Alloys and Comp.* **591** 58
[11] Hossain A, Sarker M S I, Khan M K R, Khan F A, Kamruzzaman M and Rahman M M 2018 *Appl. Phys. A* **124** 608
[12] Prakash K, Arun T, Srihari V, Jean-Marc G and Joseyphus R J , 2016 *J. Appl. Phys.* **120** 123906
[13] Bai Y, Yue W, Xiaopan L and Ronghai Y 2018 *Nanomaterials (Basel)* **8** 154
[14] Richter R and Eschrig H 1988 *J. Phys. F: Met. Phys.* **18** 1813
[15] Masudat K, Hamada N, Terakur K and Phys. J 1984 *F: Met. Phys.* **14** 47
[16] Zhang H, Punkkinen M P J, Johansson B, Hertzman S and Vitos L 2010 *Phys. Rev.* B **81** 184105
[17] Clark S J, Segal M D, Probert M J, Pickard C J, Hasnip P J and Payne M C 2005 *Zeitschrift für Kristallographie,* **220** 567
[18] Segall M D, Lindan P J D, Probert M J, Pickard C J, Hasnip P J, Clark S J and Payne M C 2002 *J. Phys. Condens. Matter* **14** 2717
[19] Payne M C, Teter M P, Allan D C, Arias T A and Joannopoulos J D 1992 *Rev. Mod. Phys.* **64** 1045
[20] Vanderbilt D 1990 *Phys. Rev.* B **41** 7892
[21] Fisher T H and Almolf J 1992 *J. Phys. Chem.* **96** 9768
[22] Monkhorst H J and Pack J D 1976 *Phys. Rev.* B **13** 5188
[23] Perdew J P, Bruke K and Ernzerhof M 1996 *Phys. Rev. Lett.* **77** 3865
[24] MacLaren J M, Schulthess T C, Butler W H, Sutton R and McHenry M 1999 *J. of Appl. Phys.* **85** 4833
[25] Liu A Y and Singh D J 1992 *Phys. Rev.* B **46** 11146
[26] Stoner E C 1939 *Proceedings of the Royal Society of London. Series A. Mathematical and Physical Sciences* **169** 372
[27] Ney J F 1957 *Physical Properties of Crystals* (Oxford: Clarendon)
[28] Zhang C, Zhang Z, Wang P, Dong J and Xing N 2007 *Solid State Commu.* **144** 347
[29] Wang H, Zhan Y and Pang M 2012 *Comput. Mater. Sci.* **54** 16
[30] Wu Z, Zhao E, Xiang H, Hao X, Liu X and Meng J 2007 *Phys. Rev.* B **76** 054115
[31] Haines J, Leger J M and Bocquillon G 2001 *Annu. Rev. Mater. Res.* **31** 1
[32] Kube C M 2016 *AIP Adv.* **6** 095209
[33] Chung D H and Buessem W R 1967 *J. of Appl. Phys.* **38** 2010
[34] Yu P Y and Cardona M 1996 *Fundamentals of Semiconductors* (Berlin: Spinger-Verlag)
[35] Dickson R M and Lyon L A 2000 *J. Phys. Chem. B* **104** 6095
[36] Oppeneer P M, Maurer T, Sticht J and Kiibler J 1992 *Phys. Rev.* B **45** 19